Stony Brook University

Effects of Processing and Medical Sterilization Techniques on 3D-Printed and Molded Polylactic Acid

A Thesis Presented

by

Mariah Nicole Geritano

to

The Graduate School

in Partial Fulfillment of the

Requirements

for the Degree of

Master of Science

in

Materials Science and Engineering

Stony Brook University

December 2015

Stony Brook University

The Graduate School

Mariah Nicole Geritano

We, the thesis committee for the above candidate for the

Master of Science degree, hereby recommend

acceptance of this thesis.

Dr. Miriam Rafailovich
Distinguished Professor, Materials Science and Engineering

Dr. Jonathan Sokolov
Professor, Materials Science and Engineering

Dr. Adriana Pinkas-Sarafova
Professor, Materials Science and Engineering

This thesis is accepted by the Graduate School

Charles Taber
Dean of the Graduate School

Abstract of the Thesis

Effects of Processing and Medical Sterilization Techniques on 3D-Printed and Molded Polylactic Acid

by

Mariah Nicole Geritano

Master of Science

in

Materials Science and Engineering

Stony Brook University

2015

Manufacturing industries have evolved tremendously in the past decade with the introduction of Additive Manufacturing (AM), also known as 3D Printing. The medical device industry has been a leader in adapting this new technology into research and development. 3D printing enables medical devices and implants to become more customizable, patient specific, and allows for low production numbers. This study compares the mechanical and thermal properties of traditionally manufactured parts versus parts manufactured through 3D printing before and after sterilization, and the ability of an FDM printer to produce reliable, identical samples. It was found that molded samples and 100% infill high-resolution samples have almost identical changes in properties when exposed to different sterilization methods, and similar cooling rates. The data shown throughout this investigation confirms that manipulation of printing parameters can result in an object with comparable material properties to that created through traditional manufacturing methods.

Dedication

This thesis is dedicated to my parents for always believing in me and my crazy ideas. I would not have the confidence to pursue my dreams if it were not for your love and support.

Table of Contents

List of Figures……..…... vi

List of Tables……..…... viii

Acknowledgements……..... ix

Chapter 1: Introduction…… 1

Additive Manufacturing……..... 1

Medical Device Development……..… 3

Poly(lactic) Acid……..... 4

Challenges of 3D Printing in Medicine……..... 6

Scope of Study……..... 7

Chapter 2: Materials and Methods……..... 8

Design and Fabrication……..... 8

Sterilization……..... 10

Characterization……..... 11

Chapter 3: Results……..... 13

Surface Analysis……..... 13

Characterization……..... 17

Chapter 4: Discussion……..... 22

Surface Structures……..... 22

Characterization……..……..... 25

Thermal Properties……..... 27

Chapter 5: Future Work and Conclusion…… 28

Future Work……..... 28

Conclusion……..... 29

Bibliography……..... 30

List of Figures

Figure 1: FDM Machine Schematic (Turner et al. 2014).....2

Figure 2: Synthesis of Polylactic Acid (Garlotta 2001).....4

Figure 3: Makerbot Replicatior 2x, Makerbot, Brooklyn USA.....8

Figure 4: Top: Standard resolution sample, Bottom: High resolution sample.....8

Figure 5: Honeycomb Structure.....9

Figure 6: Molded PLA tensile sample.....9

Figure 7: Sample loaded onto the Instron 5542.....11

Figure 8: Scanning Electron Micrograph of a flat 3D printed surface with a checkerboard pattern printed on top.....13

Figure 9: (Top) Molded samples decreasing in magnification L-R (Bottom) High Resolution 3D Printed samples decreasing in magnification L-R 5KV; High, Medium, and Low Mag, respectively.....14

Figure 10: Molded PLA scaffolds under varying sterilizations, 1 μm scale.
(a) unsterilized, (b) ethanol, (c) UV, (d)EtOH/UV.....15

Figure 11: SEM Images of various printing and sterilization conditions.
(L: Standard resolution, R: High resolution).....16

Figure 12: Contact angle data for PLA molded and printed samples under various conditions.....18

Figure 13: Thermal images of 30% infill high resolution block L- Immediately after drilling R- 1 second after drilling.....19

Figure 14: Average temperature as a function of time of PLA samples post-drilling.....20

Figure 15: Thermal images selected from the beginning and end of a sample print.....21

Figure 16: Sharkskin produced versus resolution quality. (Top: Standard, Bottom: High) (Miller et al. 2004) 22

Figure 17: 90-degree print orientation of samples.....25

Figure 18: Contact angle effect for hydrophilic (left) and hydrophobic (right) materials.....26

List of Tables

Table 1: Young's moduli in Megapascals; various conditions.....17

Table 2: Cooling rates of PLA samples.....20

Acknowledgements

It is a true honor to acknowledge the contributions from those that have supported me throughout my graduate studies and helped to make the success of this project possible. First and foremost, thank you to Dr. Miriam Rafailovich for her support throughout the many years I have spent at Stony Brook University. My success is in a large part due to her contagious passion for the field and genuine kindness.

Thank you to the Garcia Center at Stony Brook University for allowing me to access the equipment needed to pursue this research, as well as teaching me the skills needed to conduct experiments.

This project is a part of a larger, overarching 3D printing study involving the work of many individuals. I would like to thank Dr. Adriana Pinkas-Sarafova, Dr. Marcia Simon, Kuan Che Feng, Michael Cuiffo, Dr. Gary Halada, Sihana Rugova,Thomas Vonortas, and Billy Blaine for their contributions to the study.

For their constant support throughout the past semester, I would also like to thank my peers in the Materials Science and Engineering Department. I'm incredibly thankful to have met you all and be surrounded with such genuinely kind and intelligent people.

Chapter 1

Introduction

Additive Manufacturing

Manufacturing industries have evolved tremendously in the past decade with the introduction of Additive Manufacturing (AM), also known as 3D Printing. Originally, this technology was developed as a means to create first iterations of products. However, since the onset of lower price point printers, 3D printing has become a means to create end use products.

Currently, the additive manufacturing market for goods and services is estimated to be about 4 billion dollars. Wohlers Associates predicts the additive manufacturing industry will reach a worldwide value of over 10 billion dollars by 2020 (Wohlers 2014).

The medical device industry has been a leader in adapting this new technology into research and development. 3D printing enables medical devices and implants to become more customizable, patient specific, and allows for low production numbers. The first recorded use of 3D printing in medical treatment of a patient in 2005. Since then, over 14% of all additive manufacturing systems sold were to the medical sector; which has subsequently increased with the development of more specialized printers and research (Wohlers 2014).

Fused Deposition Modeling (FDM), the additive manufacturing technology explored in this study, accounts for about half of the additive manufacturing market. FDM was developed in the late 1980's by the co-founder of Stratasys, Scott Crump. Stratasys had a monopoly on the

specific technology until the patent recently expired, causing an influx of new companies developing and selling FDM machines at lower price points (Stratasys 2015).

FDM uses plastics including polymers and composites, which account for over 80% of materials sales in the Additive Manufacturing industry. Primarily, amorphous thermoplastics such as Polylactic Acid (PLA), and Acrylonitrile butadiene styrene (ABS) are used to create the filament material (Tymrak et al. 2014).

Fused Deposition Modeling (FDM) is one of the most common methods of additive manufacturing. Figure 1 shows a schematic of a typical FDM machine model (Turner et al. 2014). The raw materials are processed into a spool of filament with specified diameter based on printer parameters (typically 1.75mm/ 3mm), and then fed into the nozzle mechanism through pinch rolling. The pressure exerted on the filament during this process typically results in small tooth marks, which may affect the quality of the final print (Agarwala et al. 1996). As the filament melts, the solid portion of the feedstock serves as a piston to propel the melted filament through the nozzle and onto the print bed. The nozzle (about 200-500 μm in diameter) moves using a gantry in the X-Y plane, while the build surface provides motion in the Z direction. Typically these machines range from $1,500-$5,000, however, the development of new additive manufacturing technologies will continue to drive the prices down. Due to the availability of low price point FDM machines,

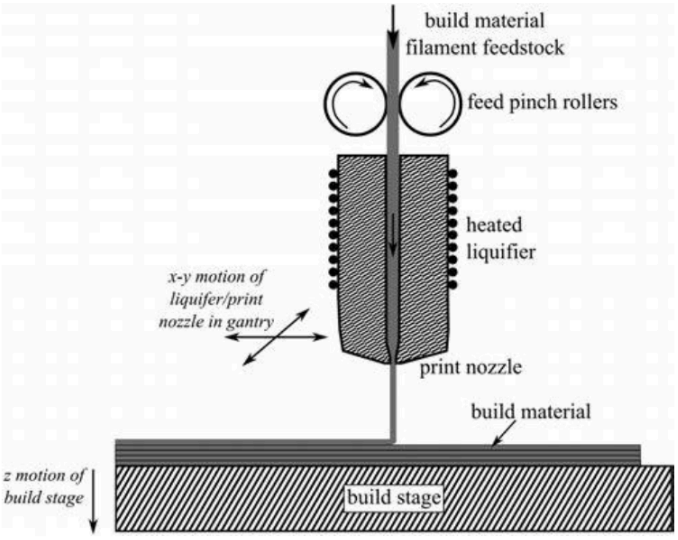

Figure 1: FDM Machine Schematic (Turner et al. 2014)

educators and hobbyists most commonly use this technology. There are also larger, industrial FDM machines in the range of $20,000-$50,000 (Ciurana et al. 2013).

While FDM continues to be a popular choice, it presents unique problems not found in other AM technologies. Amorphous thermopolymers absorb moisture from their surrounding environment if not properly stored in an airtight container. The moisture vaporizes as the filament is pushed through the extrusion nozzle, which leads to morphological and chemical malformations in the final product. In addition, bubbles and bulges in the filament cause blockages in the nozzle (Turner 2015).

Medical Device Development

Traditionally, medical devices such as prosthetics and implants are created via metal/ plastic injection molding and mechanical processing such as machining, casting, and grinding. After manufacturing, they are coated with biocompatible coatings to increase life, minimize body rejection, and possible drug eluting applications (SME 2015). Although this field has become refined through research, there still is a need for more personalized and cheaper implants. For instance, a typical modular total knee replacement implant can cost a patient approximately $32,000, and still may need to be altered during surgery. Companies produce a finite number of implant types for a specific body part, and it is up to the surgeons to select the implant most likely to fit the patient; not necessarily guaranteeing a perfect match.

Additive manufacturing has the potential to meet those needs through specialized software and medical grade 3D printers. For example, manufacturers are able to upload a CT scan onto proprietary software, which will then model the outer contour of the bone, and create a workable CAD file. Finite Element Analysis is used to select the proper materials and specific designs

based on the patient's lifestyle, and specific medical history. The final product is printed, ultimately at a lower cost than traditional methods, due to the minimized labor force and waste production.

Polylactic Acid

Polylactic Acid (PLA) is one of the leading polymers used in the creation of medical devices. PLA is well regarded for it's biodegradable and compostable components. Figure 2 depicts the two methods of polymerization to fabricate PLA with various molecular weights. The first process begins with condensation polymerizing lactic acid to create a low molecular weight, brittle, glassy polymer. This product is highly unusable for most applications due to impurities, water molecules, and the low concentration of reactive end-groups. (Garlotta 2001) Alternatively, lactide can be collected, purified, and ring-open polymerized to directly produce high molecular weight PLA. The third and final option, lactic acid and a catalyst can be azeotropically dehydrated in a high-boiling, refluxing, aprotic solvent with low pressure to create average weight PLA (weight > 300,000 Da).

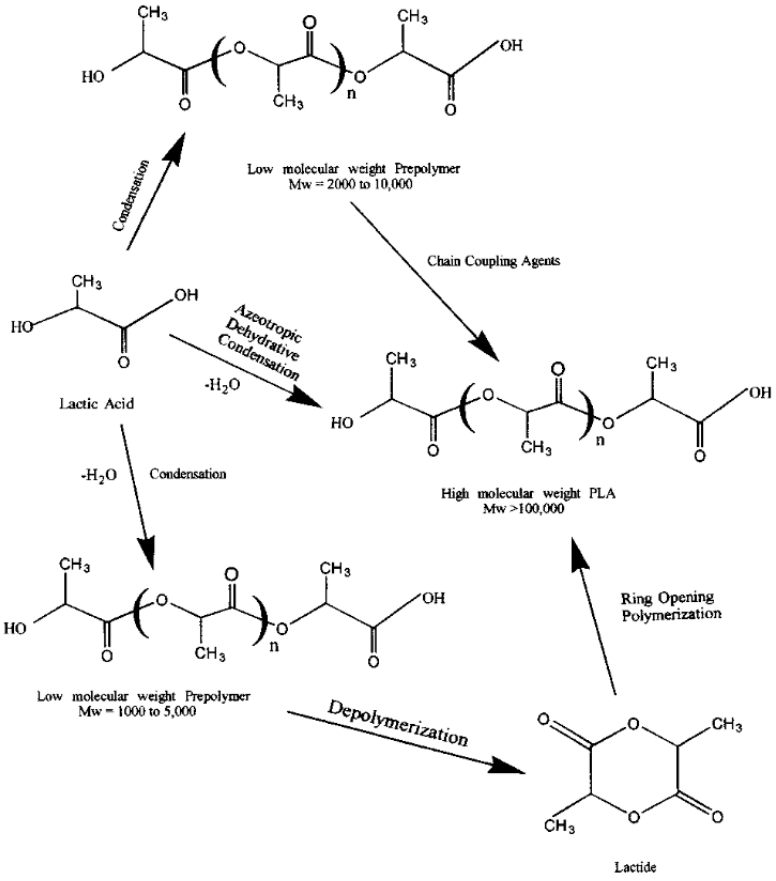

Figure 2: Synthesis of Polylactic Acid (Garlotta 2001)

PLA is known for it's high-modulus, high-strength, and thermoplastic properties that make it an ideal material for 3D printing filament. The melting point for the material is 150-180 °C, and glass transition temperature between 60-65°C (Natureworks 2015). Mechanically, bulk PLA has a Young's Modulus of approximately 3.5 Gpa. High molecular weight PLA, such as the material used to create the 3D printing filament, is naturally colorless, glossy, and stiff at room temperature. As the plastic becomes more amorphous, it can be dissolved in chlorinated solvents, tetrahydrofuran, benzene, as well as many others (Garlotta 2001).

The medical field has used PLA for medical devices before the introduction of 3D printing, due to its biocompatible and bio-absorbable nature. When PLA enters the body, simple hydrolysis of the ester backbone yields non-harmful and non-toxic compounds that can be processed by the body (Hamad 2015). In 1993, Dr. Bergsma and his team published work involving the creation of bone plates and screws for use in zygomatic fracture reconstruction using re- absorbable poly(L-lactide). The study found that the fractures were able to heal undisturbed, and encouraged bone healing around the implanted part. The degradation process was tracked over a time span of 3 years using hydrolytic activity markers, which lead to the finding that the PLA plates and screws disintegrate into crystal-like fragments of various sizes as patient cells proliferated. All patients exhibited localized swelling, but no reactions were severe enough to evoke removal of the implants (Bergsma et al. 1993).

In addition, PLA composites were used to create scaffolds to carry rhBMP2, a recombinant bone morphogenic protein, to be implanted into a patient to induce bone growth. The PLA scaffolds were able to sufficiently hold the protein in place, resulting in deposition of a collagen matrix with enchondral formation within 7 days, and bone formation within two weeks of implantation (Chang et al. 2007).

Challenges of 3D Printing in Medicine

Recent media has highlighted the great strides additive manufacturing has made within the medical field. However, much is left to be studied concerning the health effects of such medical devices compared to their traditionally manufactured counterparts. An optimal material for medical devices is biocompatible, and retains its mechanical properties after exposure to human tissue.

Medical device legislation has also played a role in the development of such products. Some key topics that have been brought to question include the proprietary protection of medical device CAD files, and quality assurance of individual devices and implants printed. The Food and Drug Administration (FDA) has held public workshops, such as the one in fall 2014, in order to provide a forum for medical device manufacturers, companies, and academic groups to provide input for future assessment methods and regulations. (FDA 2014) The FDA has approved approximately 86 3D printed medical devices on a case- by- case basis, and has recently approved a 3D printed prescription pill for patient consumption. While standardized U.S. regulations have not been formally announced, the FDA has announced plans to release such standards in the future.

Scope of Study

In 2013, 29% of all AM systems were used to create end products; creating a need to fully understand the effects of this manufacturing method on the final product (Wohlers 2013). This study compares the mechanical and thermal properties of traditionally manufactured parts versus parts manufactured through 3D printed before and after sterilization, and the ability of an FDM printer to produce reliable, identical samples. Comparisons will be made through mechanical, chemical, and surface examination.

Chapter 2

Materials and Methods

Design and Fabrication

Experimental and control samples were created using MakerBot Natural PLA (1.75 filament diameter) manufactured by NatureWorks LLC (batch number 82219).

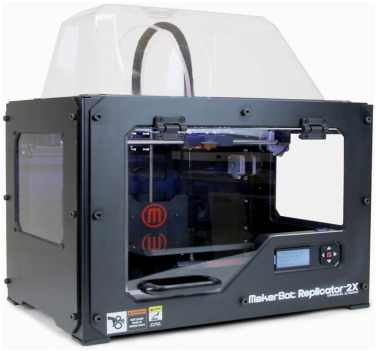

Figure 3: Makerbot Replicator 2x Makerbot, Brooklyn USA

Manufacturer specifications state that the filament has a glass temperature of 60°C, a melting temperature of 150-160 °C, and an optimal extrusion temperature of 230 °C. The study was completed with a Makerbot Replicator 2x (Makerbot Industries, Brooklyn, USA) using Makerware version 2.4.1 (Figure 3). 3D Printed samples were designed using SolidWorks software using ASTM standard specifications. Once designed, files were exported as .STL files and sliced using MakerBot's proprietary software, MakerWare. Rafts (a base of low resolution printed PLA) for the objects were added to the print to lower the risk of sample damage when removing them from the build plate. In addition, tensile samples were printed on a 90° orientation.

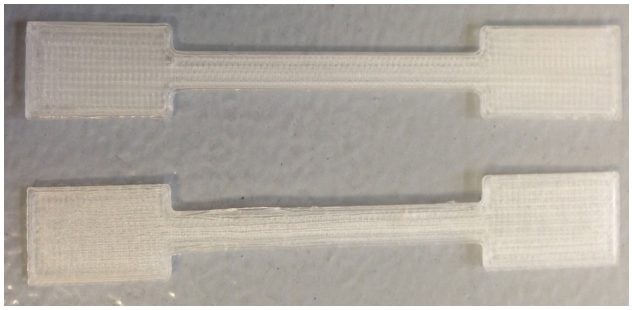

Figure 4: Top: Standard resolution sample
Bottom: High resolution sample

The first part of the study explored the different resolutions and infill parameters the Makerbot 2x hardware and software could facilitate. Samples were printed using high resolution

(.10 mm layer thickness), and standard resolution (.35 mm layer thickness), using the default 10% infill, and later 100% infill. Figure 4 shows the visible raster lines of standard and high resolution. Since the samples were thin, the infill parameter did not significantly change the appearance, weight, or measurements of the sample. Blocks with the dimensions 15mm x 20mm x 20mm were also designed and printed at high resolution with the following infill percentages: 30, 80, and 100. The Makerbot software creates a honeycomb structure within the object for infill values less than 100%, as shown in figure 5.

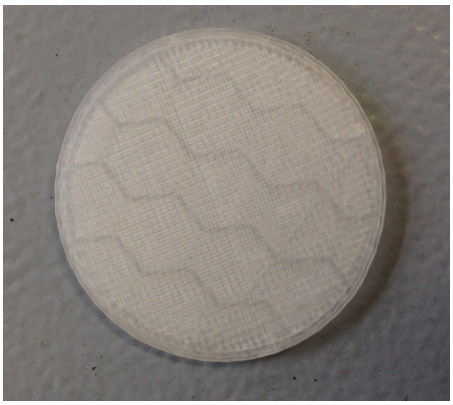

Figure 5: Honeycomb Structure

Before each print, the printing bed was leveled, blue painters tape was laid down for ease of sample removal, and the extruder was checked for any filament interferences.

An in-house molding process was used to mimic the traditional molding procedure used to create current medical devices and prosthetics. The same filament material used for 3D printing was used to create the samples by first mechanically altering the filament to ~20mm strips, increasing surface area and allowing the filament to fit into ASTM approved aluminum molds. In order to study the thermal properties of the printer, an additional mold was created in conjunction with the department machine shop with the dimensions 15mm x 20mm x 20mm.

The Carver heat press was first preheated to 180°C. Molds were prepared by sandwiching the filled molds between two pieces of Kapton polyimide film, which serve as an insulator and a means for creating flat surfaces. Once the heat press

Figure 6: Molded PLA tensile sample

reached operating temperature, the mold was placed onto the heated plates with no applied pressure for 10 minutes. After the initial melting period passed, 5 tons of pressure was placed onto the mold for 15 minutes. Pressure was relieved, and the mold was then removed from the heat press. The sandwiched mold was then placed on a cooling rack for 15 minutes, and the samples were then removed from the molds with care as to not damage the surfaces. Figure 6 shows a completed, ASTM standard molded PLA tensile sample.

Sterilization

Ethylene Oxide Gas

Samples were delivered to the Stony Brook University hospital to be treated with ethylene oxide gas in a gas diffusion sterilizer. The sterilizer was set to 71% humidity at 55 °C. The cycle time for sterilization was approximately 16 hours and 40 minutes. This includes the time of exposure and degassing of the samples.

UV-A

Samples were placed in an enclosed area approximately 16 cm under a UV-A lamp and left for 4 hours with an exposure of 120 microwatts/cm^2.

Ethanol

A bath of 70% Ethanol solution was placed under a fume hood, and samples were allowed to soak for 4 hours. Samples were then allowed to air dry in the hood before storage overnight.

Ethanol + UV-A

Samples were first placed in a bath of 70% Ethanol, allowed to soak for 4 hours. Immediately after, they were placed in an enclosed area approximately 16 cm under a UV-A lamp and left for 4 hours with an exposure of 120 microwatts/cm^2.

Characterization

Scanning Electron Microscopy (SEM)

A LEO 1550 Scanning Electron Microscope (SEM) was used to analyze the surface of the molded and 3D printed samples with exposure to sterilization. EDAX was also used to view surface impurities post printing.

Tensile Testing

The stress/ strain relationships of the printed and molded samples were compared using an Instron 5542 materials tester machine, as shown in Figure 7. Both sterilized and unsterilized samples were tested, and stresses versus strain curves were derived. Through this data, Young's Modulus was obtained.

Figure 7: Sample loaded onto the Instron 5542

Contact Angle

Contact angles of the sterilized printed and molded samples were recorded using a CAM 200 Optical Contact Angle Meter. A single drop of deionized (DI) water was placed onto the

surface of each sample, and the angle was determined using the optical camera software. Multiple readings on each sample were taken.

Thermal Images

A Nobel Biocare dental drill and a FLIR thermal imaging camera were used to observe the heat dissipation and cooling within 3D printed and molded block samples. While filming, a 2mm surgical implant medical drill created a hole in the block sample and was then removed from the block while it was allowed to cool to room temperature. Printed blocks with 30%, 80% and 100% infill and a molded block were tested. In addition, the thermal imaging system was used to view the thermal properties of the MakerBot nozzle as it was extruding filament and the cooling of the object being printed simultaneously.

Chapter 3

Results

Surface Analysis

Figure 8 is a Scanning Electron Micrograph of a cross-sectioned 3D print consisting of a flat surface with a checkerboard pattern printed directly on top in high resolution. This image was taken during a preliminary surface study previous to the work done with sterilized samples to better understand how different structures print. The scale on the graph is 100 µm, taken at 120x magnification using the rutherford backscattering spectrometry detector. There are two very distinct patterns on the sample differing in roughness, shape, and orientation. In the base of the material, the material appears to be homogeneous. However, the cross-sectional cut, showed vertical shale-like layers, along with deformities within the base.

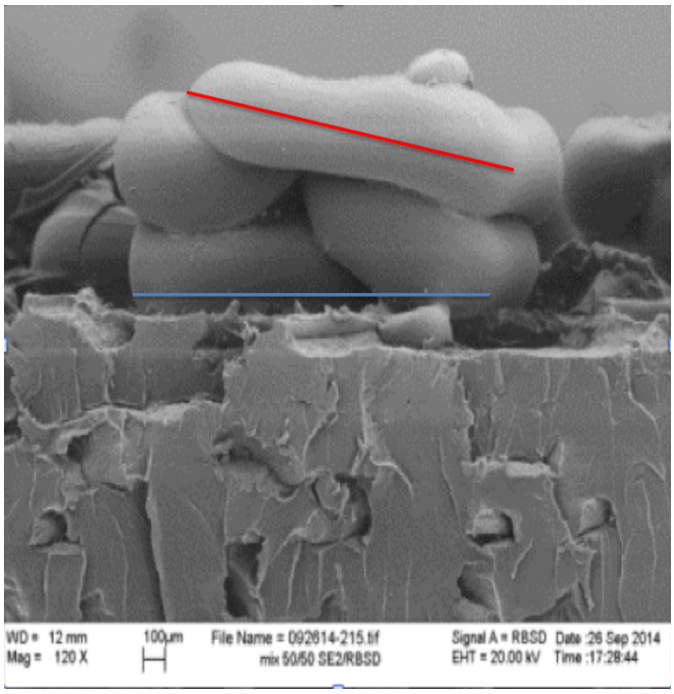

Figure 8: Scanning Electron Micrograph of a flat 3D printed surface with a checkerboard pattern printed on top.

The grid structure was designed on CAD software to be solid. However, in the center of the structure, there is a gap approximately 230 µm in length. The blue line indicates the length of the individual grid structure (1.60 mm), and the red line signifies the length of one "layer" of the structure (1.46 mm). The spaces between each individual grid structure has evidence of nano-

and micro- structures not put into the original CAD design; they are considered artifacts of the 3D print.

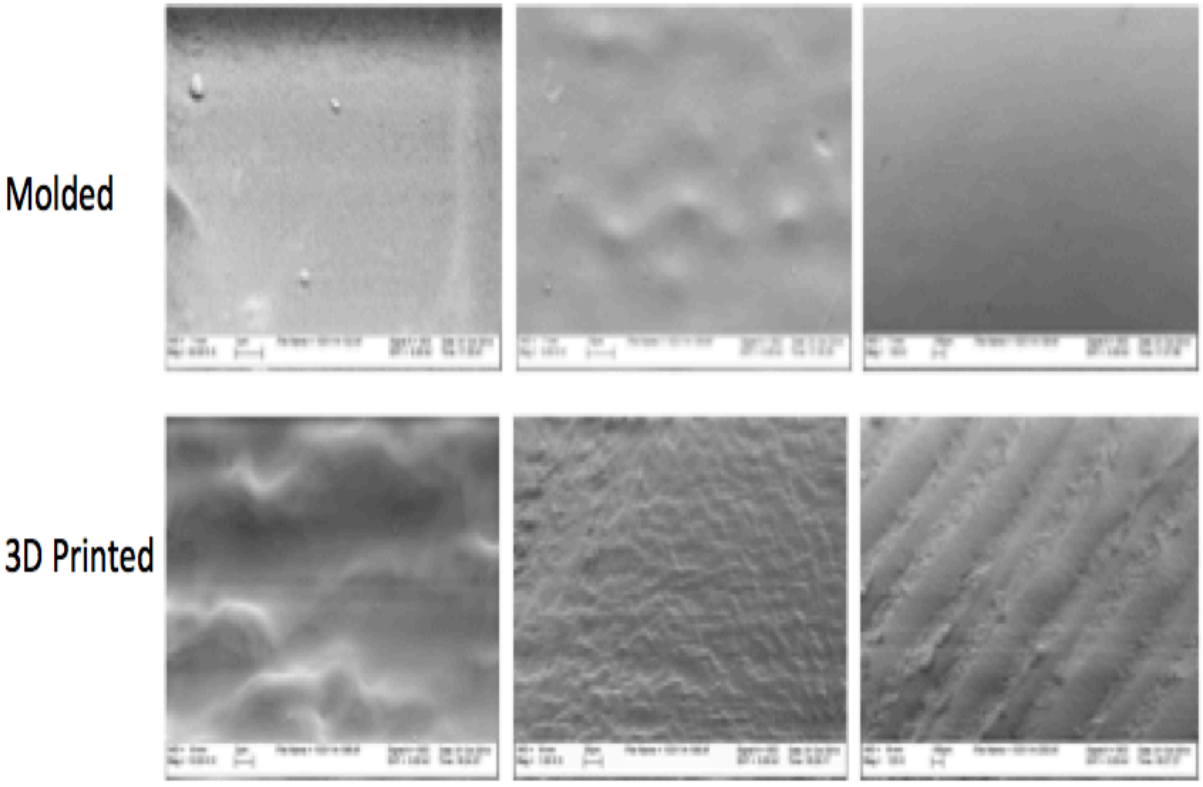

Figure 9: (Top) Molded samples decreasing in magnification L-R
(Bottom) High Resolution 3D Printed samples decreasing in magnification L-R
5KV; High, Medium, and Low Mag, respectively

Figure 9 shows the topological differences of molded samples and samples 3D printed at high resolution. The molded samples show minimal surface roughness at low magnification, with manufacturing defects presenting as waves on the sample at medium magnification. High magnification reveals artifacts on the surface about .5 μm in length, as well as cracking throughout the image. The 3D printed samples have distinct raster structures on low magnification ranging from approximately 100 μm to 200 μm. The medium magnification focused on the top of one of the rasters. The extrusion process causes the rough pattern, or

sharkskin. When imaged on high magnification, the valleys and peaks of the sharkskin become more prominent and there is evidence of micro- and nano- topography.

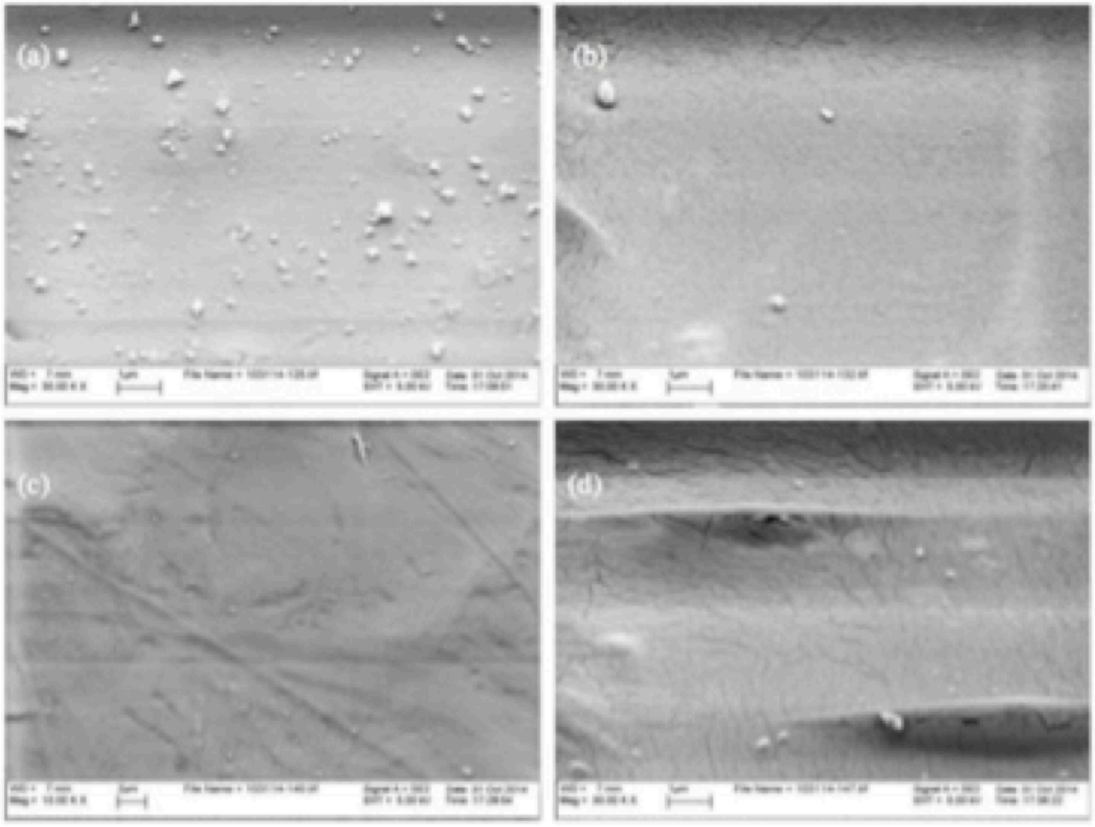

Figure 10: Molded PLA scaffolds under varying sterilizations, 1 μm scale. (a) unsterilized, (b) ethanol, (c) UV, (d) EtOH/UV

Traditionally molded samples were first exposed to standard sterilization methods, as shown in Figure 10. The unsterilized sample has evidence of environment contamination of metals and other polymers (white objects on sample). The ethanol (EtOH) washes away the loose particles, leaving the original PLA surface mostly clean. However, small cracks were visible on the surface. UV treated samples were free from foreign artifacts, but appeared to have scratches on the surface, and a more varied topography caused by the molding process. Finally, the EtOH/UV treated sample showed the most dramatic physical change. It shows the more prominent hills and valleys consistent with a non-perfect molding system, and evidence of

contamination. Cracks across the sample are also visible, with some small pieces peeling away from the sample.

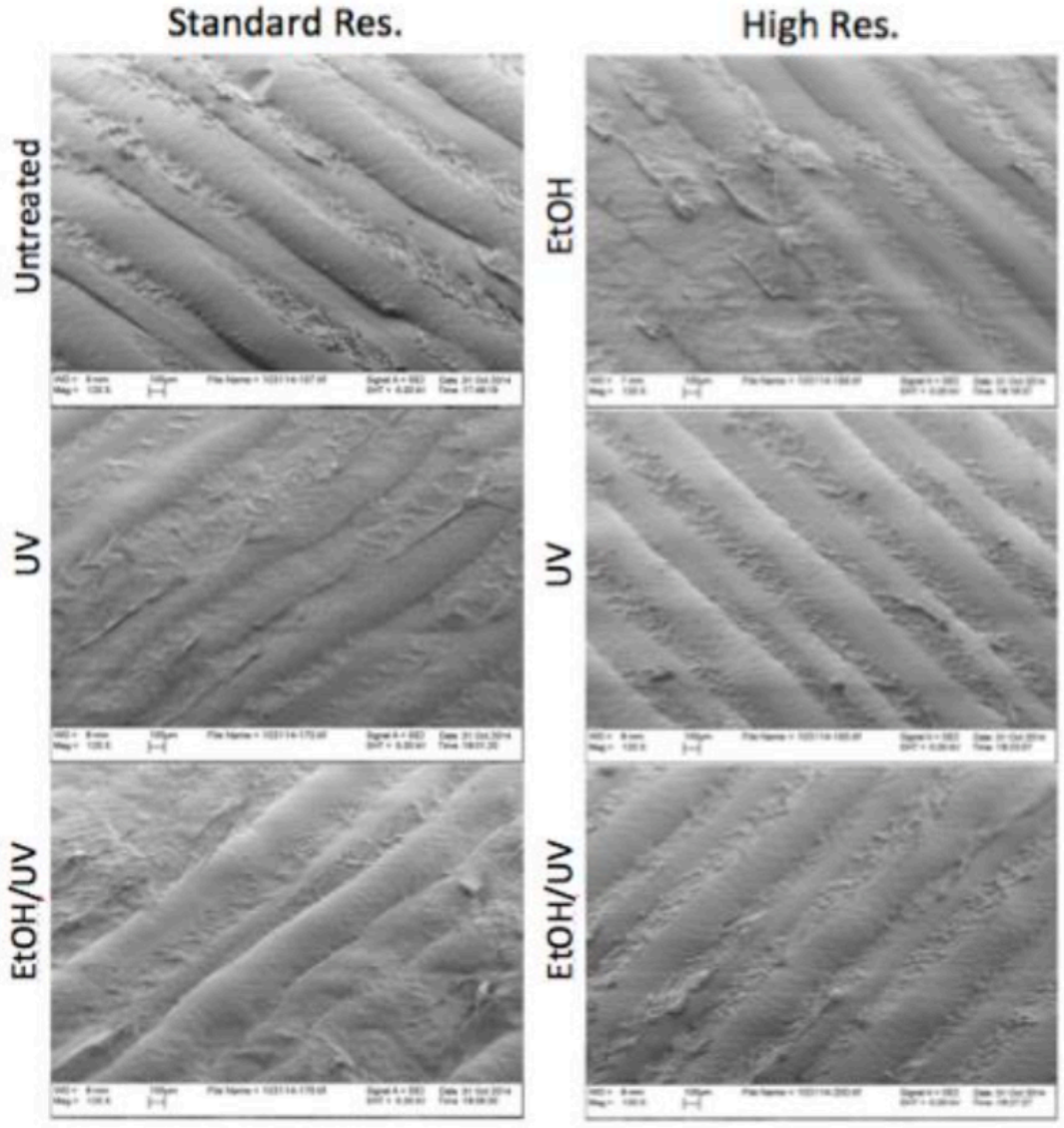

Figure 11: SEM images of various printing and sterilization conditions. (L: Standard resolution, R: High resolution)

High resolution and standard resolution samples were subjected to ethanol, UV, and Ethanol/UV sterilization treatments and imaged. Surface results are shown in Figure 11. All samples have a typical distinct printing pattern, alternating 100 and 200 μm filament raster

structures. The 70% ethanol treated sample appears to have printing deformities on the surface of the 3D printed surfaces. Both standard and high resolution samples treated with ethanol and ethanol/UV show deformities on the surface.

Characterization

Tensile Testing

Tensile tests were conducted on both molded and printed samples exposed to different sterilization methods, with and without 24 hours soaking in cell media. Stress versus strain curves were compiled, and Young's modulus was calculated for each condition, as shown in Table 1.

	Printed (MPa)		**Molded (MPa)**	
	No Media	Media	No Media	Media
Untreated	1129		1117	
EtOH	1847	1742	1368	1330
UV	1762	1690	1342	1292
EtOH/UV	1815	1724	1256	1117
E.O.	1370		1279	

Table 1: Young's moduli in Megapascals; various conditions

The 3D printed PLA samples had a significantly higher Young's modulus than their molded counterparts. The addition of media (to mimic an in vivo environment) yielded a lower Young's modulus. Sterilization had a larger effect in the printed samples, but the Young's moduli for each mode of sterilization were similar in number.

Contact Angle

Different modes of processing can lead to material properties causing altered behaviors of the surrounding environment. Contact angle is an important tool to help understand how 3D printing affects how the body will respond to printed PLA. Figure 12 summarizes a contact angle study done with 5 different sterilization methods molded and printed at 100% infill in standard and high resolution. All conditions showed the largest increase in contact angle when treated with ethylene oxide gas. Ethanol had that largest effect on the molded samples, bringing the contact angle from 58 ° to 67 °. UV treatment increased the contact angle for both the molded and high resolution samples, but decreased the contact angle on the standard printed samples. The combined ethanol and UV treatment brought the molded sample contact angle from 58° to 65°, and increased the high resolution sample slightly from 61° to 63°. However, the treatment lowered the contact angle measurement of the standard samples from 75° to 65°.

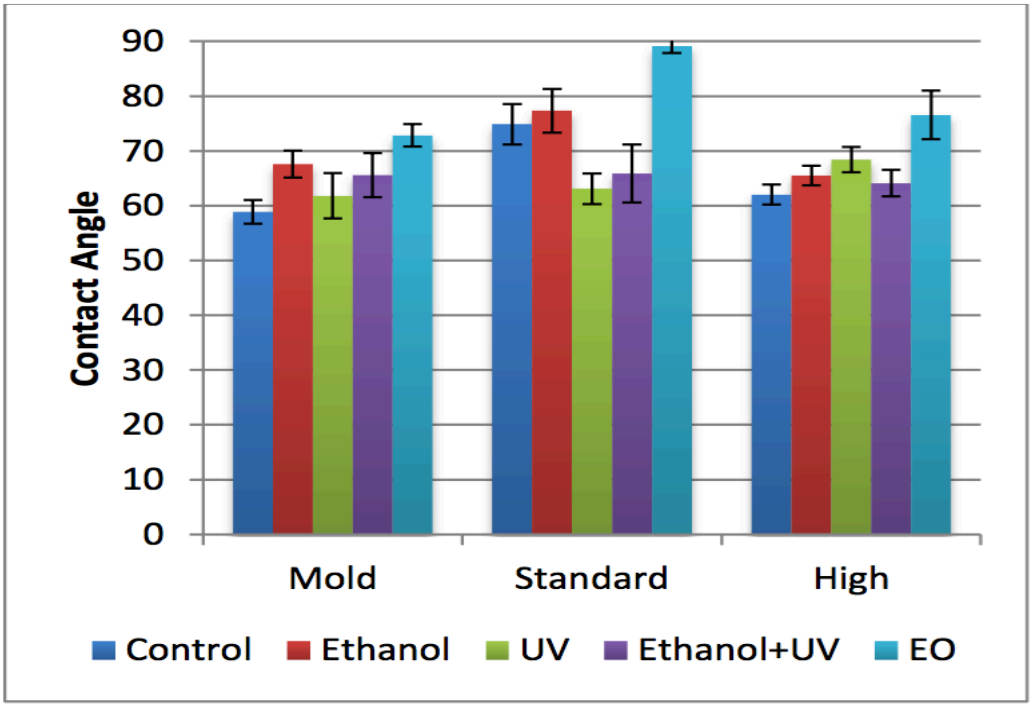

Figure 12: Contact angle data for PLA molded and printed samples under various conditions

Thermal Analysis

It is important to explore the thermal properties of materials used in the human body, especially those that are candidates for bone replacements. The process of 3D printing repeatedly heats and cools a polymer, which can change it's crystalline structure and ultimately it's material properties. By demonstrating the cooling curve of 3D printed versus molded PLA, we can compare processing effects. Figure 13 shows a general example of heat dispersion within PLA blocks after being drilled into using a professional grade dental drill. Different colors correspond to temperatures as per the color scale on the right hand side of each image, with white representing the highest intensity, and black representing the lowest. These images are screen shots taken from time lapse videos used to extract the data for cooling rate calculations. The 30% infill samples printed at high resolution, had the highest rate of heat dissipation when compared to the other samples. Immediately after drilling, the block's center dropped from 150 °C to 83 °C. The other samples displayed a lower temperature drop, decreasing from 150 °C to about 105 °C. Molded samples and the 100% infill high resolution samples displayed the most similar cooling rates.

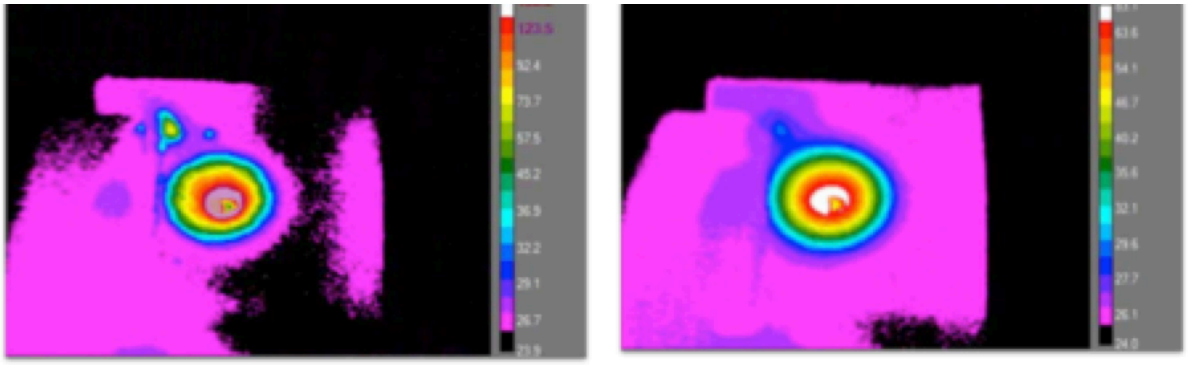

Figure 13: Thermal images of 30% infill high resolution block
L- Immediately after drilling R- 1 second after drilling

The cooling process was recorded beginning at time 0 (immediately after drilling), to 40 seconds for 5 conditions. The heat dissipation rate was calculated using the slopes of each sample, which allow us to confirm the cooling patterns viewed through the thermal camera videos.

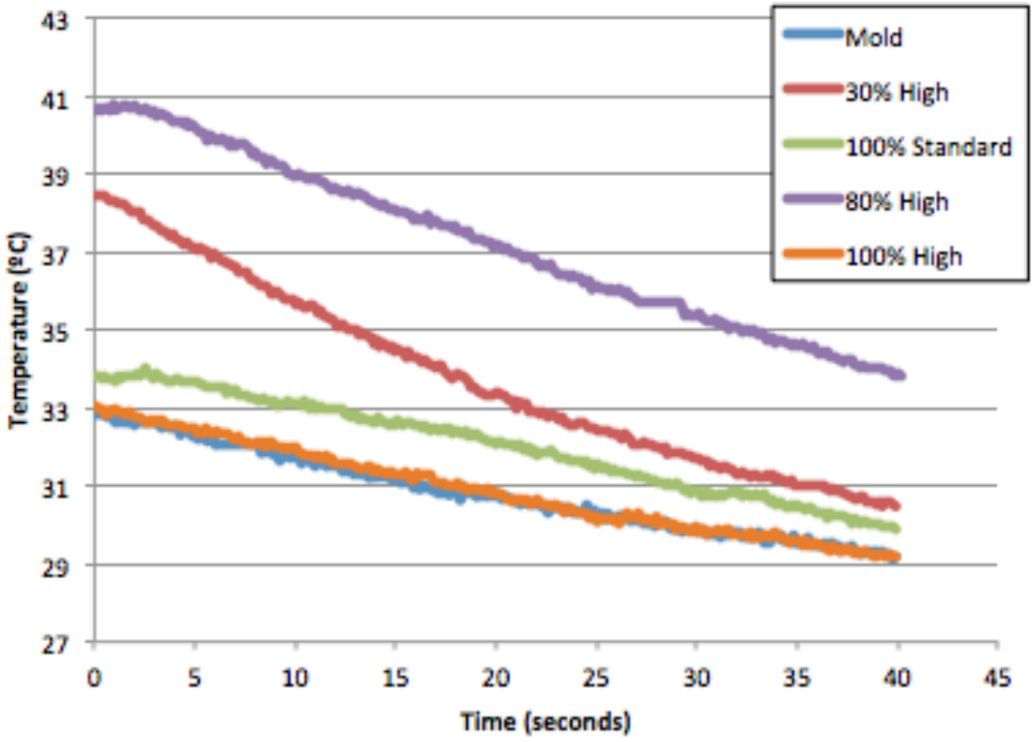

Figure 14: Average temperature as a function of time of PLA samples post-drilling

Condition	dT/dt (ºC/sec)	R^2
30% Fill	-0.20	0.9761
80% Fill	-0.18	0.9958
100% Standard	-0.11	0.9939
100% High	-0.10	0.9882
Molded	-0.09	0.9841

Table 2: Cooling rates of PLA samples

Figure 14 and Table 2 both display the slopes as the change in temperature (degrees Celsius) over time (seconds). The high resolution 30% infill had the highest heat dissipation rate of .20 °C per second, followed by high resolution 80% infill with a rate of .18° C per second. The final three, 100% standard resolution, 100% high resolution, and molded samples had similar rates of .11, .10. and .09 °C per second, respectively.

The thermal camera was also used to capture temperature profiles of the 3D printer nozzle, and the object printed during the printing process, and immediately afterwards. The test object was a cylinder with measurements of 5mm height, and a 2.5 mm diameter. Figure 15 shows select images from the video, capturing the temperature profiles at the beginning and end of the print. Temperature readings higher than 150°C could not be recorded because those values exceeded the capacity of the thermal camera. During extrusion, the nozzle maintained a steady temperature above 150°C. After extrusion, the PLA is cooled immediately to approximately 130°C, thus solidifying quickly.

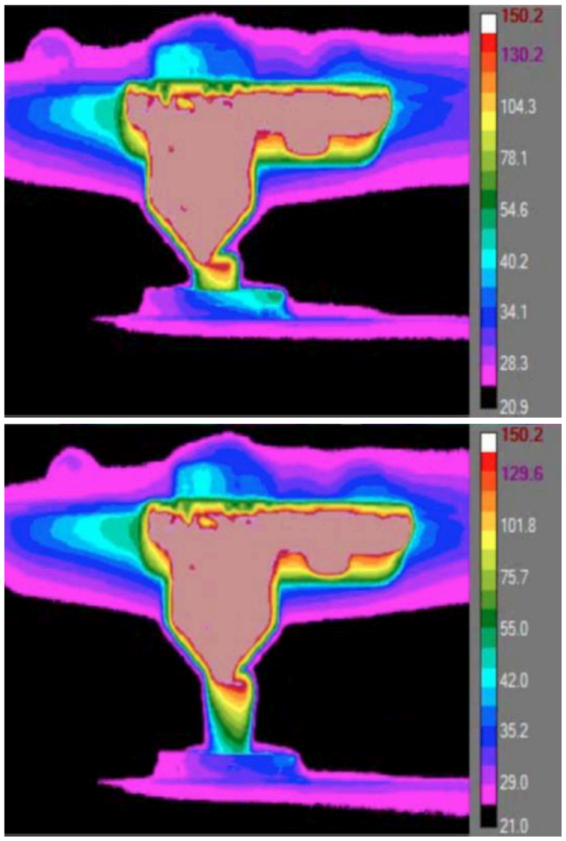

Figure 15: Thermal images selected from the beginning and end of a sample print.

Chapter 4

Discussion

Surface Structures

The structures in Figure 8 played an important role in the initiation of this study. The top and bottom have distinct features, which could be the result of a difference in rate of convective heat loss, or the gradient temperature of the filament as it was extruded through the nozzle. The bottom layer shows little evidence of extrusion lines, suggesting the nozzle was at a higher temperature when printing. The top layer demonstrates little cohesion between the extruded filament. This could also be the function of the nozzle diameter. A smaller nozzle diameter would allow for greater detail and resolution of a sample. The nozzle opening plays an important role in print quality as well. A smaller nozzle diameter allows for greater resolution, which would decrease the visible filament lines seen in the grid portion of the print and decrease the amount of sharkskin produced.

The base of the flat layer structure is textured with microstructures that were not part of the inherent CAD design. These structures are very similar to the material phenomenon sharkskin. Sharkskin is a result of capillary action of the filament leaving the nozzle as it's being heated and extruded. (Nithi-Uthai 2003) The high local stress

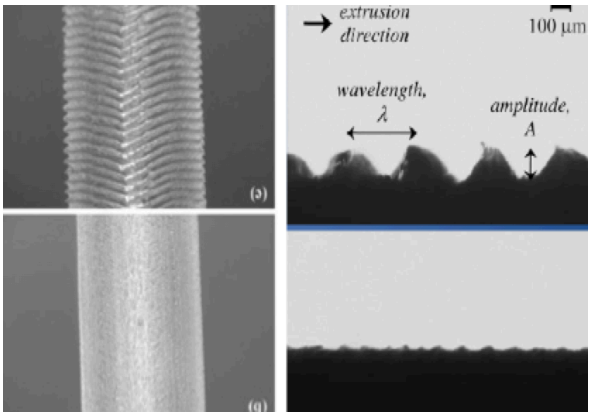

Figure 16 : Sharkskin produced versus resolution quality. (Top: Standard, Bottom: High)
(Miller et al. 2004)

located at the tip of the nozzle results in a strong deformation of the PLA chains and a large tensile stress. It appears as though the nozzle is "sputtering" material due to these periods of stress relaxation and stress growth resulting in micro-waves on the object's surface. Higher resolution objects show less evidence of the sharkskin phenomenon, as shown by Figure 16.

When comparing 3D printed samples to molded samples, one of the most prominent differences is the surface texture. When a sample is molded, heat is applied to melt the material and create a smooth surface. When done in an industry setting, the processing is typically automatic, thus creating a smooth surface on the nano-scale level. However, our process involved a Carver heat press that requires manual application of pressure. If pressure isn't applied evenly throughout the surface, or does not remain constant for the prescribed period of time, imperfections such as the waves seen under medium magnification can occur. The artifacts seen under high magnification is a result of the lab environment.

Cracking that was present under high magnification could be a function of polymer cooling post- molding. If a crystalline polymer is cooled too fast, the outer crystalline layer puts a large amount of stress on the inner amorphous layer, causing warping and a decrease in stress-crack resistance. Sink marks or notches on the surface are also by-products of rapid cooling.

The 3D printed samples have a very distinct ridge (raster) pattern due to filament extrusion while printing. The rasters appear throughout the surface of the sample, and alternate between 200 um micron and 100 micron. In between these ridges is evidence of sharkskin of varying measurements. Upon closer magnification, 3D printed samples have different texture patterns on the top of the raster than the spaces in between each raster. The medium and high magnifications are focused on the top of one of the rasters.

The sterilization methods used were those already approved for medical grade sterilization on traditionally molded implants. As such, there should not be any significant changes on the surfaces after sterilization. The unsterilized sample showed a high number of artifacts due to the unsterilized processing environment. The treated samples showed a reduction in such artifacts, however, some were still visible on the surface. In addition, the surface cracking is more distinct on the ethanol/ UV treated samples, indicating they have grown in depth. The sample also began to peel due to the UV treatment immediately following the ethanol treatment, exacerbating the sterilization effects. Samples treated with only ethanol showed the smallest change in surface structure as compared to the unsterilized, with very few artifacts. 70% ethanol is a liquid at room temperature, and can easily clear the surface of artifacts not native to the material.

All sterilization methods affected the surfaces in a very mild manner; however, none exhibited a drastic change in surface structure. The ethanol treatment had the most noticeable effect, appearing to deteriorate the print pattern on the sample surfaces. UV showed to have a flattening effect on the surfaces.

In addition, for 3D printing machines to be usable in the medical field, reliability is a key factor. The final object must match the output file from the CAD software, which requires ease of information transfer between the design software and hardware of the printer. Once a CAD file is created, it can be imported and exported numerous times through different editing and slicing software before it reaches the printer. If a file is not transferred correctly due to software incompatibility, the output could contain defects, such as missing slices in the object or micro artifacts such as those found in the samples. These microstructures could be the result of such miscommunication. If they go unnoticed in the final print, the end product could lead to

complications within the patient because of a change in cell metabolic activity. The user must be able to control the complete output of the machine by ensuring reproducibility.

Characterization

Bond strength between the layers of materials, which is derived from the energy of cohesion, plays an important role in strength of the sample. For example, print orientation of the sample can change the young's modulus of the same object. Our samples were printed at an orientation that created 90-degree angle print lines. (Figure 17) Many of the standard resolution samples fractured outside the acceptable area of fracture, which could be a result of the visible raster lines. These lines were less apparent on the surface of the high resolution samples, which were the most successful during tensile testing. Due to the higher resolution and 100% infill, the voids created by raster patterns decreased, diminishing the effects of print orientation.

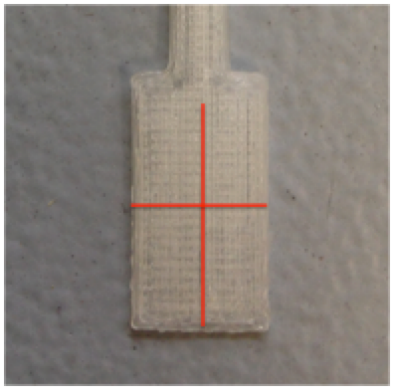

Figure 17: 90-degree print orientation of samples

The 3D printed samples displayed a higher young's modulus, suggesting 3D printing creates a more brittle structure than traditional molding processes. Again, this could be the function of printing orientation. Molded samples contain no voids, thus creating one homogeneous object, as opposed to an object with visible voids and raster lines. When exposed to media, both sample sets saw a decrease in modulus values, indicating the transition to a more elastic material. This is in part due to PLA's biodegradability properties. When exposed to water in the media, the PLA begins to erode and become more amorphous. Within the media, there are

proteins that can attach to the cell surface, which could cause surface defects. However, there were no enzymes that would lead to an alteration of properties. Overall, the ethanol treatment caused the largest increase in moduli.

Based on the contact angle, inferences can be made as to how the extracellular matrix and cells will react when exposed to such material. More hydrophilic samples have smaller contact angle measurements less than 90° (Figure 18). Most materials used for medical purposes have low contact angles because the material is favorable for cell adherence. Our data suggests that ethylene oxide gas treatment alters the contact angle the greatest. Since ethylene oxide is a gaseous treatment, there must be a period of degassing for the sample. This period of time can differ depending on the structure and material of material being sterilized. Since this is a novel processing method, there have been no previous studies suggesting a specified protocol for 3D printed items. Therefore, degassing time could have influenced the contact angle. The 70% Ethanol treatment showed a slight increase in contact angle, which could be the result of residual water in the pores of the printed samples, since ethanol has a rapid evaporation rate. UV treatment resulted in a higher contact angle in both the molded and high resolution samples, but a decrease in the standard resolution. UV light is known to cross-link polymers, which would form a more homogeneous sample than the visible porous structure of the standard resolution. The UV brought the contact angle of the standard resolution sample to an almost identical value of the control molded and high resolution samples,

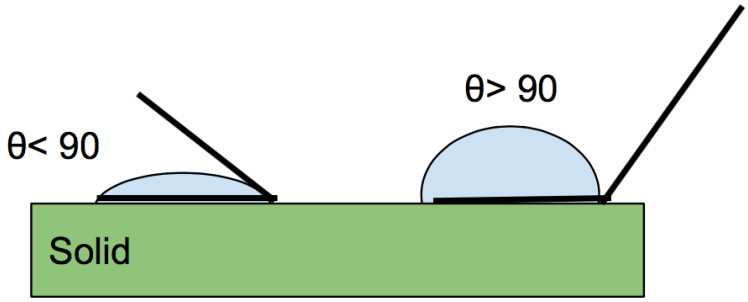

Figure 18: Contact angle effect for hydrophilic (left) and hydrophobic (right) materials

suggesting cross linking occurred. The combination ethanol and UV treatment lead to a contact angle approximately halfway between the ethanol treated samples and UV treated samples.

The changes in contact angle throughout the sterilization study bring up an interesting method of personalization for future 3D printed medical implants. If manufacturers are able to control hydrophobicity, and even structural changes such as crosslinking using different forms of standard sterilization, implants can be modified for various end uses without incurring any extra production costs.

Thermal Properties

Based on the calculated heat loss rates, the 30% infill high- resolution samples cooled the fastest. These values can be used to make inferences about the thermal diffusivity values and recrystallization of each sample. Since the infill was at a low percentage, the internal structure of the object may have for heat to escape more quickly than it's 100% infill and molded counterparts. When inserted into a living organism, the internal structure will be occupied with other organic elements.

These more dense samples have the lowest cooling rate, which is in line with the effects of recrystallization during traditional processing. The molded and high-resolution parts would play a more beneficial role in total part replacement over a longer period of time, while the standard printed and smaller infill percentages would be favorable for smaller implants that encourage native cell regeneration.

In addition, since this was done in an open room with airflow, heat was lost due to convection from the air in the build environment as well as conduction to the surface below. In an enclosed environment, more accurate data could be extrapolated.

Chapter 5

Future Work and Conclusion

Future Work

Data collected from this study provided an initial overview of material properties as a function of processing, allowing for future experiments to continue exploring differences between molded and FDM 3D printed samples. Through the experiments carried out in this thesis, we now understand the level of sterilization and enclosed environment needed to obtain samples most similar to those comparable to current medical implants and devices.

In addition to the array of tests used in this study, charpy impact testing would prove to be beneficial to better understand how sterilized material would function under conditions similar to those experienced in high impact areas of the body. Differential Scanning Calorimetry (DSC) should be conducted to compare the phase transition temperatures of the processed filament compared to the bulk PLA pellets used more commonly in industry. Processing material as simply as extruding to form a filament, and then extruding out of a heated nozzle could affect crystallization and thermodynamic properties.

The study utilized a Makerbot Replicator 2x, a basic desktop printer with relatively low-resolution precision as compared to current advertised medical 3D printers on the market. Still, using this printer for further experimentation through parameter manipulation can prove to be useful. Current medical 3D printers use a different 3D printing technology to produce implants and samples, but are often far more expensive.

3D printing is a unique manufacturing technique due to its dependence on both hardware, and software to control the final print. The defects and sharkskin found on the samples must be investigated further to find the ultimate cause, and learn how to control these micro- and nano-structures. A more in depth study of the nozzle thermodynamics would give great insight on the effects extrusion has on the crystallization and cooling rate of the polymer. By perfecting a more affordable technology such as fused deposition modeling, personalized implants can become accessible to a greater population.

Conclusion

This study was executed to explore a novel fabrication method for medical devices and implants. Fused deposition modeling processing has a small impact on the tensile strength of an object, creating a more brittle structure. Molded samples and 100% infill high-resolution samples have almost identical changes in properties when exposed to different sterilization methods, and cooling rates. Both processing methods are comparable, however, there still needs to be further investigation on the micro- and nano- structures within 3D printed samples, which seem to be inherent in the FDM technology. The data shown throughout this investigation confirms that manipulation of printing parameters can result in an object with comparable material properties to that created through traditional manufacturing methods.

Bibliography

Afrose, Mst Faujiya, S.h. Masood, Mostafa Nikzad, and Pio Iovenitti. "Effects of Build Orientations on Tensile Properties of PLA Material Processed by FDM." *AMR Advanced Materials Research* 1044-1045 (2014): 31-34. Web.

Agarwala, Mukesh K., Vikram R. Jamalabad, Noshir A. Langrana, Ahmad Safari, Philip J. Whalen, and Stephen C. Danforth. "Structural Quality of Parts Processed by Fused Deposition." *Rapid Prototyping Journal* 2.4 (1996): 4-19. *Emerald Insight*. Web.

Basulto, Dominic. "Why It Matters That the FDA Just Approved the First 3D-printed Drug." *Washington Post*. The Washington Post, 11 Aug. 2015. Web. 17 Nov. 2015.

Bergsma, Eelco J., Fred R. Rozema, Ruud R.m. Bos, and Wim C. De Bruijn. "Foreign Body Reactions to Resorbable Poly(l-lactide) Bone Plates and Screws Used for the Fixation of Unstable Zygomatic Fractures." *Journal of Oral and Maxillofacial Surgery* 51.6 (1993): 666-70. Web.

Bergsma, J.e., F.r. Rozema, R.r.m. Bos, G. Boering, and W.c. De Bruijn. "Late Degradation Tissue Response to Poly(l-lactide) Bone Plates and Screws." *The Biomaterials: Silver Jubilee Compendium* (1995): 101-07. Web.

Bonda, David J., Sunil Manjila, Warren R. Selman, and David Dean. "The Recent Revolution in the Design and Manufacture of Cranial Implants." *Neurosurgery* (2015): 1. Web.

Chang, Po-Chun, Bu-Yuan Liu, Cheng-Meei Liu, Hsin-Hua Chou, Ming-Hua Ho, Hwa-Chang Liu, Da-Ming Wang, and Lein-Tuan Hou. "Bone Tissue Engineering with Novel RhBMP2-PLLA Composite Scaffolds." *Journal of Biomedical Materials Research Part A J. Biomed. Mater. Res.* 81A.4 (2007): 771-80. Web.

Ciurana, Joaquim De, Lídia Serenóa, and Èlia Vallès. "Selecting Process Parameters in RepRap Additive Manufacturing System for PLA Scaffolds Manufacture." *Procedia CIRP* 5 (2013): 152-57. Web.

Dobircau, Larisa, Nicolas Delpouve, Romuald Herbinet, Sandra Domenek, Loïc Le Pluart, Laurent Delbreilh, Violette Ducruet, and Eric Dargent. "Molecular Mobility and Physical Ageing of Plasticized Poly(lactide)." *Polym Eng Sci Polymer Engineering & Science* 55.4 (2014): 858-65. Web.

"FDM Technology." *FDM*. Stratasys, 2015. Web. 18 Nov. 2015.

Garlotta, Donald. "A Literature Review of Poly(Lactic Acid)." *Journal of Polymers and the Environment* 9.2 (2001): 63-84. Web.

Hamad, K. "Properties and Medical Applications of Polylactic Acid: A Review." *Expresspolymlett Express Polymer Letters* 9.5 (2015): 435-55. Web.

"Materials Safety Data Sheet." *Encyclopedia of Lubricants and Lubrication* (2014): 1-9. *PLA 3D Printer Filament/ MakerBot PLA*. NatureWorks. Web.

Miller, Erik, and Jonathan P. Rothstein. "Control of the Sharkskin Instability in the Extrusion of Polymer Melts Using Induced Temperature Gradients." *Rheologica Acta Rheol Acta* 44.2 (2004): 160-73. Web.

Nithi-Uthai N, Manas-Zloczower I: Numerical Simulation of Sharkskin Phenomena in Polymer Melts, Appl. Rheol. 13 (2003) 79.

Nofar, Mohammadreza, Alireza Tabatabaei, and Chul B. Park. "Effects of Nano-/micro-sized Additives on the Crystallization Behaviors of PLA And PLA/CO2 Mixtures." *Polymer* 54.9 (2013): 2382-391. Web.

Serra, Tiziano, Miguel A. Mateos-Timoneda, Josep A. Planell, and Melba Navarro. "3D Printed PLA-based Scaffolds." *Organogenesis* 9.4 (2013): 239-44. Web.

Turner, Brian N., and Scott A. Gold. "A Review of Melt Extrusion Additive Manufacturing Processes: II. Materials, Dimensional Accuracy, and Surface Roughness." *Rapid Prototyping Journal* 21.3 (2015): 250-61. *Emerald*. Web.

Tymrak, B.m., M. Kreiger, and J.m. Pearce. "Mechanical Properties of Components Fabricated with Open-source 3-D Printers under Realistic Environmental Conditions." *Materials & Design* 58 (2014): 242-46. Web.

"U.S. Food and Drug Administration." *Public Workshop*. FDA, 2014. Web. 17 Nov. 2015.

"What Is Medical Manufacturing?" *SME*. N.p., 2015. Web. 18 Nov. 2015.

"Wohlers Report 2013." *Wohlers Report 2013*. Wohlers Associates, 2013. Web. 03 Dec. 2015.

"Wohlers Report 2014." *Wohlers Report 2014*. Wohlers Associates, 2014. Web. 03 Dec. 2015.